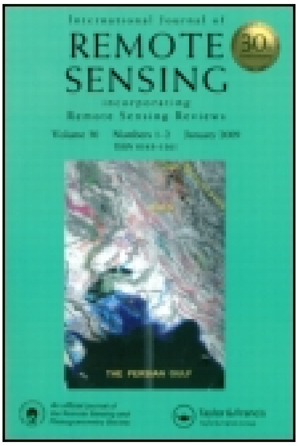

International Journal of Remote Sensing

Publication details, including instructions for authors and subscription information:
http://www.tandfonline.com/loi/tres20

On the net surface water exchange rate estimated from remote-sensing observation and reanalysis

Ali Behrangi[a], Sun Wong[a], Kaniska Mallick[b] & Joshua B. Fisher[a]

[a] Jet Propulsion Laboratory, California Institute of Technology, Pasadena, California, USA

[b] Centre de Recherche Public - Gabriel Lippmann, Département Environnement et Agro-biotechnologies (EVA), Belvaux, Luxembourg

Published online: 04 Mar 2014.

International Journal of Remote Sensing, 2014
Vol. 35, No. 6, 2170–2185, http://dx.doi.org/10.1080/01431161.2014.889866

Taylor & Francis
Taylor & Francis Group

On the net surface water exchange rate estimated from remote-sensing observation and reanalysis

Ali Behrangi[a]*, Sun Wong[a], Kaniska Mallick[b], and Joshua B. Fisher[a]

[a]*Jet Propulsion Laboratory, California Institute of Technology, Pasadena, California, USA;* [b]*Centre de Recherche Public – Gabriel Lippmann, Département Environnement et Agro-biotechnologies (EVA), Belvaux, Luxembourg*

(*Received 20 November 2013; accepted 25 January 2014*)

This study compares the net surface water exchange rates, or surface precipitation (*P*) minus evapotranspiration (ET), and atmospheric water vapour sinks calculated from various observations and reanalyses, and investigates whether they are physically consistent. We use the observed precipitation from the Global Precipitation Climatology Project (GPCP) and the Tropical Rainfall Measuring Mission (TRMM) 3B43, ocean evaporation from Goddard Satellite-based Surface Turbulent Fluxes Version 2c (GSSTF2c), and land ET from the Moderate Resolution Imaging Spectroradiometer (MODIS) global ET project (MOD16) and PT-JPL products to calculate observed *P* minus observed ET. *P*–ET is also obtained from atmospheric water vapour sink calculated using Atmospheric Infrared Sounder (AIRS)/Advanced Microwave Sounding Unit observation specific humidity observation and wind fields from the Modern-Era Retrospective Analysis for Research and Applications (MERRA) and ERA-interim, denoted as $\mathrm{AIRS_M}$ and $\mathrm{AIRS_E}$, respectively. MERRA and ERA-interim water vapour budgets are also calculated for cross-comparison and consistency check. The period of study is between 2003 and 2006 based on the availability of all of the data sets. Averaged water vapour sinks from AIRS and reanalysis are consistent over the global ocean and are close to zero (range: 0.02–0.06 mm day^{-1}), but range between 0.14 and 0.23 mm day^{-1} when land is included. Over ocean within 50°S–50°N, averaged observed *P* minus observed evaporation shows a much larger negative number than that obtained from AIRS and reanalysis. The differences mainly occur over subtropical oceans, especially in the southern hemisphere in summer and the northern hemisphere in winter. Over land, generally higher agreement between observed *P* minus observed ET and atmospheric water vapour sinks (calculated from AIRS and reanalysis) is found. However, large regional differences, often with strong seasonal dependence, are also observed over land. Estimates of atmospheric water vapour sinks are influenced by both winds and biases in water vapour data, especially over tropics and subtropical oceans, thereby calling for the need for further investigations and consistency checks of satellite-based and reanalysis water vapour, reanalysis winds, *P* observations, and surface evaporation estimates. In higher latitudes, atmospheric water vapour sinks calculated from $\mathrm{AIRS_M}$, $\mathrm{AIRS_E}$, MERRA, and ERA-interim are more consistent with each other.

1. Introduction

Atmospheric and surface branches of the hydrologic cycle are connected through the net surface water exchange or surface precipitation (*P*) minus evapotranspiration (ET). An

*Corresponding author. Email: ali.behrangi@jpl.nasa.gov

excess of evaporation to P over oceans ultimately leads to the amount of freshwater that is transported through the atmosphere and precipitated over continental regions. Accurate quantification of P–ET plays an important role in the calculation of the land-atmosphere water balance (e.g. Trenberth et al. 2007; Syed et al. 2007) and is critical for understanding the changes in the global hydrologic and energy cycle (through latent heat release) in a changing climate (e.g. Allen and Ingram 2002; Dai, Fung, and Del Genio 1997; Sun et al. 2007; Stephens et al. 2012). For example, drought has been showing an increasing trend since the 1970s (Dai, Trenberth, and Qian 2004), which is likely a combined effect of decreased P in the tropical and subtropical land as well as increased atmospheric demand due to the warming (Trenberth et al. 2007). Accurate estimation of P and ET, together with other components of the hydrologic cycle, is also critical for many applications such as water resources management, agricultural planning, and prediction of natural hazards.

Remote-sensing instruments and techniques have allowed local to global observation of P and ET from space (e.g. Adler et al. 2003; Huffman and Bolvin 2012; Xie and Arkin 1997; Anderson et al. 2007; Mu et al. 2007; Fisher, Tu, and Baldocchi 2008; Mallick et al. 2009). As ground measurement of P and ET is limited to a few locations, mainly over land, global evaluation of remote-sensing observations remains challenging. Despite great efforts to improve remote-sensing products from space, our current P and ET estimates are still subject to large bias and uncertainties (Tian et al. 2007; Tian and Peters-Lidard 2010; Vinukollu et al. 2011). Owing to the lack of spatiotemporally complete ground measurement of precipitation, Tian and Peters-Lidard (2010) computed measurement spread from an ensemble of six different quasi-global merged precipitation products to estimate uncertainties without relying on any reference data. Their uncertainty maps show that there are large regional and seasonal uncertainties in the estimation of precipitation, especially over high latitudes where snow and light rainfall are dominant and often missed by current precipitation products (e.g. see Behrangi et al. (2012)). Adler, Gu, and Huffman (2012) used a similar approach to identify bias and uncertainties in global precipitation climatology products including the widely used Global Precipitation Climatology Project (GPCP; Adler et al. 2003; Huffman and Bolvin 2012). They also conclude that precipitation bias and uncertainty are the largest over ocean and high latitudes. Although the error analysis using an ensemble of several products is a reasonable approach, errors can be underestimated as the merged precipitation products are not completely independent and typically share several level-2 products. Similar to P, the quantification of global ET has long been associated with large uncertainties owing to different parameterization schemes used to develop these ET products. The LandFlux-EVAL project aims to evaluate and compare different newly developed ET data sets. Comparing IPCC AR4 GCM simulations with satellite data sets, Mueller et al. (2011) found a high level of uncertainty (inter-quartile ranges) in most regions. While quantifying the uncertainty of multiple ET products over the conterminous USA, Ferguson et al. (2010) found that the choice of vegetation parameterization, followed by surface temperature, has the greatest impact on remote-sensing-based ET uncertainty. Additional uncertainty (4–18%) was also reported to be stemmed from different sources of net radiation.

Recognizing the challenge in error analysis of P and ET in lack of sufficient ground observations, here we use a different approach using independent data sets to assess the net surface water exchange (or P–ET) instead of individual P and ET. Independent estimate of P–ET is obtained from the column-integrated water vapour sinks from Atmospheric Infrared Sounder/Advanced Microwave Sounding Unit (AIRS; Divakarla et al. 2006; Fetzer et al. 2004; 2006; Susskind et al. 2006) observations as well as two reanalysis products (Wong, Fetzer, Tian, et al. 2011 and Wong, Fetzer, Kahn, et al. 2011). The column-integrated water vapour sink is equal to the net surface water exchange using the following budget equation (e.g. Peixoto and Oort 1992; Syed et al. 2007; Trenberth, Fasullo, and Mackaro 2011; Wong, Fetzer, Kahn, et al. 2011):

$$P - E = -\int_{p_1}^{p_n} \left(\frac{\partial q}{\partial t} + u\frac{\partial q}{\partial x} + v\frac{\partial q}{\partial y} + w\frac{\partial q}{\partial z} \right) \frac{\mathrm{d}p}{g},$$

where P is precipitation, E is surface evaporation, t is time, q is specific humidity, (u, v, w) are wind velocities along x, y, and z directions, p_1 is the top of the atmosphere pressure, p_n is the surface pressure, and g is the gravitational constant. In this study, we choose p_1 = 200 hPa, above which water vapour concentration is negligible in contributing to column integration.

Wong, Fetzer, Kahn, et al. (2011) compared $P-E$ and atmospheric water vapour sinks from different observation-based data sets and Modern-Era Retrospective Analysis for Research and Applications (MERRA) reanalysis over the oceans in 50°S–50°N and documented the discrepancies among data sets in seasonal averages and variability. In the present study, we extend the work of Wong, Fetzer, Kahn, et al. (2011) by including observation ET data over lands and expand the investigated region to higher latitudes for a globally complete analysis of total P–E. We will also test the sensitivity of using different reanalysis winds combined with the latest version of AIRS water vapour data for the budget calculations.

The comparative analysis of the net quantity from the two independent approaches will be reported and discussed using zonal plots and geographical maps to identify regions of main differences that could be useful for future research and improvement of the individual products. The analysis is also helpful to investigate whether the current products are consistent to close the atmospheric branch of the hydrologic cycle. Description of the data sets used in this study is presented in Section 2. Section 3 includes the results and discussion followed by concluding remarks in Section 4.

2. Data and processing

2.1. *Precipitation*

Precipitation data are obtained from the latest version of monthly Global Precipitation Climatology Project (GPCP V2.2; Adler et al. 2003; Huffman and Bolvin 2012) and the Tropical Rainfall Measuring Mission (TRMM) 3B43 V7 (Huffman et al. 2007) products. GPCP data is obtained from the World Meteorological Organization's World Data Center at The National Oceanic and Atmospheric Administration's National Climatic Data Center. TRMM 3B43 V7 is obtained from the Goddard Earth Sciences Data and Information Services Center (GES DISC). The monthly GPCP product provides global long-term precipitation data at 2.5° × 2.5° grids by merging rain data from gauges and space-borne sensors, including Special Sensor Microwave/Imager (SSM/I), geostationary, and polar orbiting infrared imagers and sounders. The GPCP merger procedure uses more-accurate estimates of precipitation (e.g. gauges over land and passive microwave) to adjust the bias in other estimates (e.g. from infrared imagers and sounders) and then combines the estimates with an inverse error weighting technique. TRMM 3B43 (hereafter referred to as T3B43) provides a single, gauge-adjusted precipitation rate per calendar month at 0.25° × 0.25° resolution between 50°S and 50°N using several high-quality microwave precipitation retrievals including the TRMM Combined Instrument (TCI), TRMM Microwave Imager (TMI), Special Sensor Microwave Imager/Sounder (SSMI/S), Advanced Microwave Scanning Radiometer for EOS (AMSR-E), Advanced

Microwave Sounding Unit-B (AMSU-B) with correction for scan angle effect (Vila, Ferraro, and Joyce 2007), and microwave-calibrated precipitation estimates from geostationary infrared brightness temperature.

2.2. *Evapotranspiration*

Observation of daily ET was obtained from three different sources. Over ocean, Goddard Satellite-based Surface Turbulent Fluxes Version 2c (GSSTF2c; Chou et al. 2003; Shie et al. 2009; Shie 2011) obtained from GES DISC is used as it has shown reliable performance and improvements compared to the previous products (Shie 2011). The GSSTF2c fluxes are produced using the up-to-date and improved input data sets, i.e. the SSM/I V6 surface/10 m wind speeds and total precipitable water, as well as the NCEP/DOE Reanalysis-2 SST, 2 m air temperature, and sea-level pressure. The product is available from July 1987 to December 2008.

Over land, monthly ET is obtained from two satellite-based products: the MOD16 (Mu, Zhao, and Running 2011) and PT-JPL (Fisher, Tu, and Baldocchi 2008). MOD16 is the official Moderate Resolution Imaging Spectroradiometer (MODIS) ET product, which is based on forward run of the Penman–Monteith (Monteith, 1965) equation. This algorithm is driven by the radiation (net radiation and ground heat flux) and meteorological variables (air temperature, T_a; vapour pressure, ea) from the NASA Global Modeling and Assimilation Office (GMAO), MODIS vegetation index (e.g. enhanced vegetation index (EVI)) (MOD13A2), and leaf area index (LAI) (MOD15A2). The characteristic feature of MOD16 is that it parameterizes the stomatal and aerodynamic conductances based on a biome property lookup table where the maximum conductances are constrained by atmospheric vapour pressure deficit and air temperature scalars. PT-JPL is found to perform favourably to MOD16 (Vinukollu et al. 2011). The PT-JPL algorithm (Fisher, Tu, and Baldocchi 2008) is based on the potential ET (PET) formulation of the Priestley–Taylor (PT) equation, which is a reduced version of the Penman–Monteith equation, eliminating the need to parameterize the stomatal and aerodynamic conductances, leaving only equilibrium evaporation multiplied by a constant (1.26), called the α coefficient. In PT-JPL, PET is reduced to ET using ecophysiological constraint functions based on net radiation, atmospheric moisture, and vegetation indices. The characteristic of PT-JPL is its simplicity, which bypasses the complex conductance parameterization, yet accommodates the environmental and biophysical control of ET. Monthly $1^o \times 1^o$ resolution MOD16 data was obtained from GES DISC. Monthly ET estimates from PT-JPL was obtained from http://josh.yosh.org/datamodels/1deg_monthlyglobalET_%201984-2006/ at a spatial resolution of $1^o \times 1^o$ resolution. Both products have been used in a wide array of applications and inter-comparisons (Mu et al. 2007; Phillips et al. 2009; Jiménez et al. 2011; Mueller et al. 2011; Zelazowski et al. 2011).

2.3. *Specific humidity and wind vectors*

The atmospheric specific humidity (q) and three-dimensional wind vectors are needed to calculate atmospheric water vapour sinks (Equation (1)). We obtained q from the latest AIRS level 3 (L3; version 6) product at $1^o \times 1^o$ horizontal resolutions and 12 AIRS standard pressure levels (Tian et al. 2013). AIRS is a hyperspectral infrared sounder aboard the Aqua spacecraft, which was launched into a polar Sun-synchronous orbit at 705 km altitude in May 2002. The ascending node of the orbit crosses the equator at approximately 1330 local time and the descending node at 0130 local time. For comparison, q is also obtained from the MERRA (Rienecker et al. 2011; Bosilovich, Robertson, and Chen 2011) and the ERA-interim (Dee et al. 2011) reanalyses and mapped on a common AIRS grid for water vapour budget calculations. ERA-interim is the latest European Centre for Medium-Range Weather Forecasting (ECMWF) global atmospheric reanalysis and MERRA uses the latest Goddard Earth Observing System (GEOS-5; Rienecker et al. 2011) to assimilate observations, including AIRS radiance data. Daily AIRS q together with daily winds from MERRA and ERA-interim are used to calculate P–ET from Equation (1). The calculations are performed on common $10^{o} \times 5^{o}$ longitude-latitude grids at 12 vertical pressure levels up to 200hPa, the topmost level where AIRS measurements are sensitive to atmospheric water vapour in the tropics (e.g. Fetzer et al. 2008; Gettelman et al. 2004). Calculation at $10^{o} \times 5^{o}$ horizontal resolution is important to alleviate issues regarding the lack of sampling in cloudy areas that can hinder the calculation of AIRS moisture gradients (Wong, Fetzer, Kahn, et al. 2011). The land fraction in each $10° \times 5°$ grid is computed from land fraction data set from a higher resolution ($0.25° \times 0.25°$). Grids with land fraction greater than 0.5 are counted as 'land' and those less than 0.5 are counted as 'ocean', when the global budgets are computed. We caution that the land-only or ocean-only budgets may change with a different threshold, but the global budget (land + ocean) and the geographical distribution of P–ET are robust results as discussed in Section 3. More precise global land-only or ocean-only budgets require data with higher spatial resolution. Another issue is related to the lack of sampling in cloudy areas and causes sampling biases in q that range from −1 to 0.5 g/kg in the lower troposphere (Yue et al. 2013) or 2–5% in the total column water vapour (Fetzer et al. 2006). For comparative analysis and consistency check, atmospheric water vapour sinks are also calculated using q and wind vectors from MERRA and ERA-interim averaged onto $10^{o} \times 5^{o}$ longitude-latitude grids at 12 vertical pressure levels. Note that MERRA and ERA-interim assimilate AIRS radiance data and produce complete q fields even in cloudy areas. Comparison between the calculation with AIRS q fields and reanalysis q fields indicates that the biases in P–ET introduced by AIRS sampling q biases are not as significant as the biases in P–ET introduced by using different reanalysis wind fields.

The study period of 2003–2006 is selected based on availability of all of the data sets. MOD16 and AIRS data became available since late 2002 and evaporation data from GSSTF2c and ET data from PT-JPL is available only up to the end of 2008 and 2006, respectively. However, the four year data set is found to be sufficient for the comparative analysis performed in this study. All data sets are converted to monthly $10^{o} \times 5^{o}$ longitude–latitude resolution maps prior to analysis.

3. Results and discussion

Figure 1 shows the climatological average of GPCP precipitation as well as ET from ET1 (combined evaporation from GSSTF2c over ocean and ET from MOD16 over land). Annual average maps are shown along with the average values for boreal summer [June–July–August (JJA)] and boreal winter [December–January–February (DJF)]. A northward shift of intense precipitation band in boreal summer and southward shift in boreal winter can be observed, which could not be distinguished in the annual average map. However, ocean evaporation maps show maximum values in the southern hemisphere in boreal summer and in the northern hemisphere in boreal winter. Although large precipitation rates can occur over land (e.g. over India and the Amazon), evaporation is typically much less over the land because of limited water availability. Use of the TRMM 3B43 and

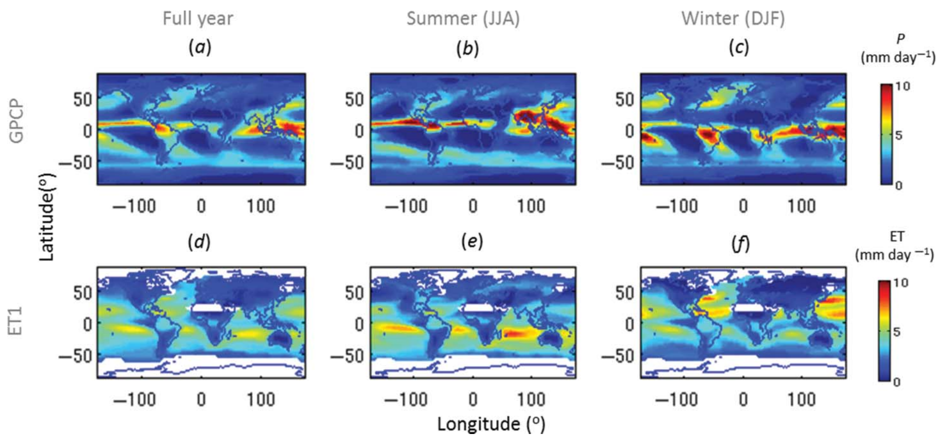

Figure 1. Maps of precipitation and ET climatological averages from GPCP and ET1. Annual, summer, and winter precipitation averages are shown in panels (*a*), (*b*), and (*c*), respectively. Similarly, the annual, summer, and winter ET1 averages are shown in panels (*d*), (*e*), and (*f*), respectively. ET1 represents the combined evaporation from GSSTF2c over ocean and ET from MOD16 over land. White colours indicate area with no data.

PT-JPL products result in fairly similar maps to those shown in Figure 1; therefore, for better comparison, maps of climatological differences are shown in Figure 2. Note that ET2 is similar to ET1, but uses PT-JPL ET data instead of MOD16. Figures 2(*a*)–(*c*) (precipitation difference maps) suggest that, compared to GPCP, T3B43 shows lower precipitation over high latitude ocean and higher precipitation over the tropical ocean. In the high latitudes (starting at latitude 40°), GPCP uses precipitation (including snow) data retrieved from the TIROS Operational Vertical Sounder (TOVS)/AIRS through regression relationships between collocated ground measurements and a few cloud-related parameters (Adler et al. 2003; Huffman et al. 2009; Susskind et al. 1997; Bolvin et al.

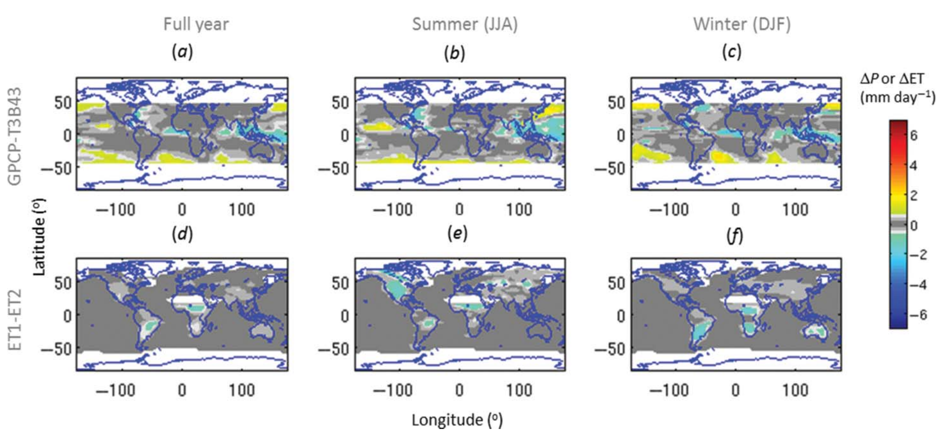

Figure 2. Maps of climatological differences between the two precipitation (GPCP minus T3B43) and ET (ET1-ET2) products. Annual, summer, and winter averages are shown in (*a*), (*b*), and (*c*) for precipitation and (*d*), (*e*), and (*f*) for ET, respectively. ET2 uses ET data from PT-JPL instead of MOD16 over land.

2009). However, T3B43 employs a collection of microwave precipitation estimates within fixed three-hour bracket times and then fills any remaining gaps with geostationary infrared rain estimates to produce spatiotemporally complete precipitation fields (Huffman et al. 2007). As discussed in Behrangi et al. (2012, Forthcoming), the current microwave and infrared instruments and associated precipitation retrieval techniques show little skill and sensitivity to retrieve light rainfall and snowfall, which are the dominant types of precipitation in high latitudes. Over land, the two precipitation products are in good agreement as both of them use rain gauge data for bias adjustment.

Figures 2(*d*)–(*f*) show that PT-JPL values are larger than MOD16 values, and the differences are seasonally dependent. This could be due to the differences in the parameterization schemes used in both products. PT-JPL uses ecophysiological functions to constrain the Priestley–Taylor parameter whereas MOD16 parameterized the atmospheric and surface conductances through a biome-specific lookup table for resolving the Penman–Monteith equation. For more detailed information pertaining to the differences between the two ET products, readers are referred to Fisher, Tu, and Baldocchi (2008) and Mu, Zhao, and Running (2011). However, the climatology differences are often less than 1 mm day^{-1}. Note that in order to facilitate cross-comparison of different maps, the same scales are used for colourbars throughout the study.

Figure 3 shows the maps of GPCP-ET1 (top row), $AIRS_M$ (middle row), and $AIRS_E$ (bottom row). $AIRS_M$ represents the value of *P*–ET calculated from Equation (1) using specific humidity (*q*) from AIRS and wind components from MERRA, whereas $AIRS_E$ uses wind vectors from ERA-interim. Therefore, $AIRS_M$ and $AIRS_E$ allow independent assessments of the observed *P* minus observed ET and sensitivity to the source of wind values. The annual, summer, and winter climatology maps show that in general high agreement exists between the three estimates to capture the seasonal and regional distribution of *P*–ET. Regions with positive *P*–ET lose water vapour through precipitation (e.g. tropical convergence zone, the west pacific, storm south America, Indian monsoon, and Amazon). In contrast, in regions with negative *P*–ET, atmosphere gains water vapour

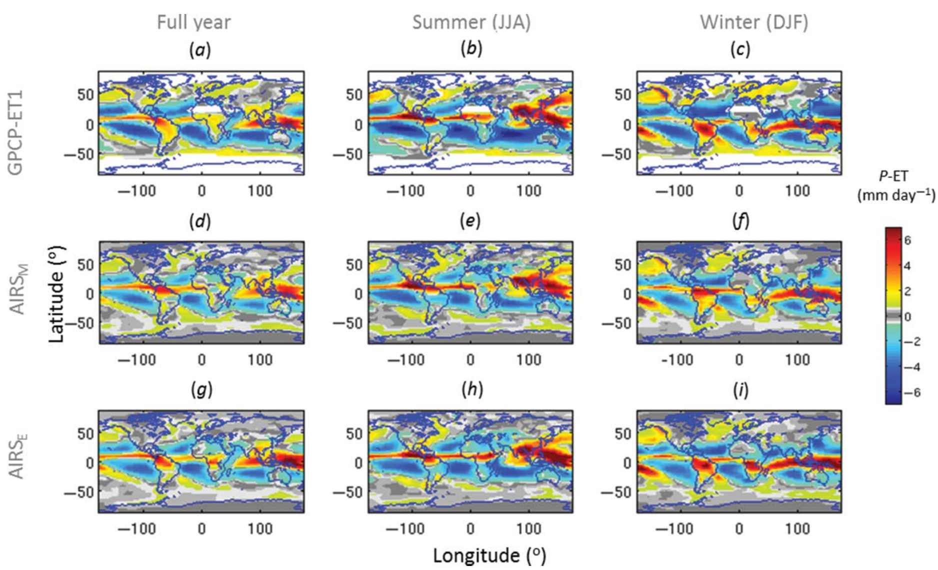

Figure 3. Maps of climatological average of *P*–ET from GPCP-ET1, $AIRS_M$, and $AIRS_E$.

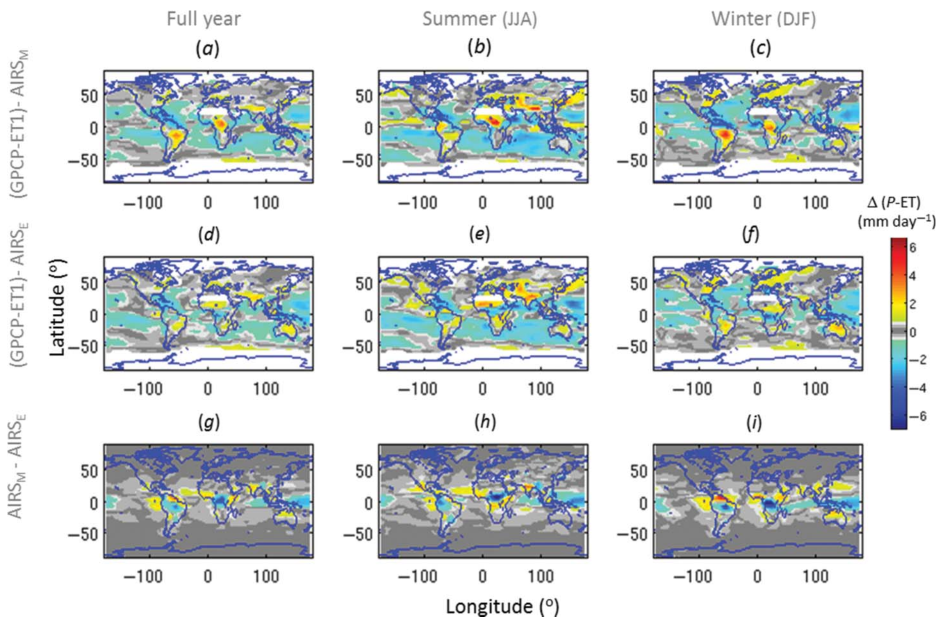

Figure 4. Maps of climatology difference between (GPCP-ET1) and $AIRS_E$, (GPCP-ET1) and $AIRS_M$, and $AIRS_M$ and $AIRS_E$.

through evaporation or ET (e.g. evaporation in subtropical oceans). A more detailed cross-comparison can be obtained using Figure 4, in which maps of climatology difference between (GPCP-ET1) and $AIRS_E$ (top row), (GPCP-ET1) and $AIRS_M$ (middle row), and $AIRS_M$ and $AIRS_E$ are displayed. Comparison of the three rows in Figure 4 shows that GPCP-ET1 has a much larger negative *P*–ET value than that of $AIRS_M$ and $AIRS_E$ over the subtropical oceans and storm tracks. In contrast, GPCP-ET1 shows larger *P*–ET over the South America continent, Australia, north of India, and the surrounding areas including part of the Tibetan Plateau and Pakistan in summer. Larger GPCP-ET1 is also observed in winter over the central South America and Africa continents, a large part of Europe, and northwest Asia. GPCP benefits from a dense gauge network over Europe, which can suggest that precipitation estimate is more reliable there. However, as discussed in Swenson (2010), GPCP might overestimate precipitation at high latitudes owing to possible overestimation of gauge undercatch. Note that the maps of $AIRS_M$-$AIRS_E$ suggest that at higher latitudes *P*–ET calculated from AIRS water vapour convergence is less affected by the differences in wind vectors from MERRA and ERA-interim compared to over the tropics; thus, the high-latitude results can be inferred to be more conclusive.

Figure 5 shows the zonal distribution of mean *P*–ET computed from $AIRS_E$, $AIRS_M$, GPCP-ET1, GPCP-ET2, T3B43-ET1, and T3B43-ET2 for annual (left column), winter (middle column), and summer (right column) over land and ocean (top row; Figures 5(*a*)–(*c*)), ocean (middle row; Figures 5(*d*)–(*f*)), and land (bottom row; Figures 5(*g*)–(*i*)). Figure 5 suggests that *P-E* from observation of *P* (either from GPCP or from T3B43) and *E* is more negative than that observed from $AIRS_E$ or $AIRS_M$ over the subtropical ocean, especially in the southern hemisphere in summer and the northern hemisphere in winter. A fraction of the differences can be related to the underestimation of light rain in the subtropical oceans from infrared and microwave instruments used in GPCP; however,

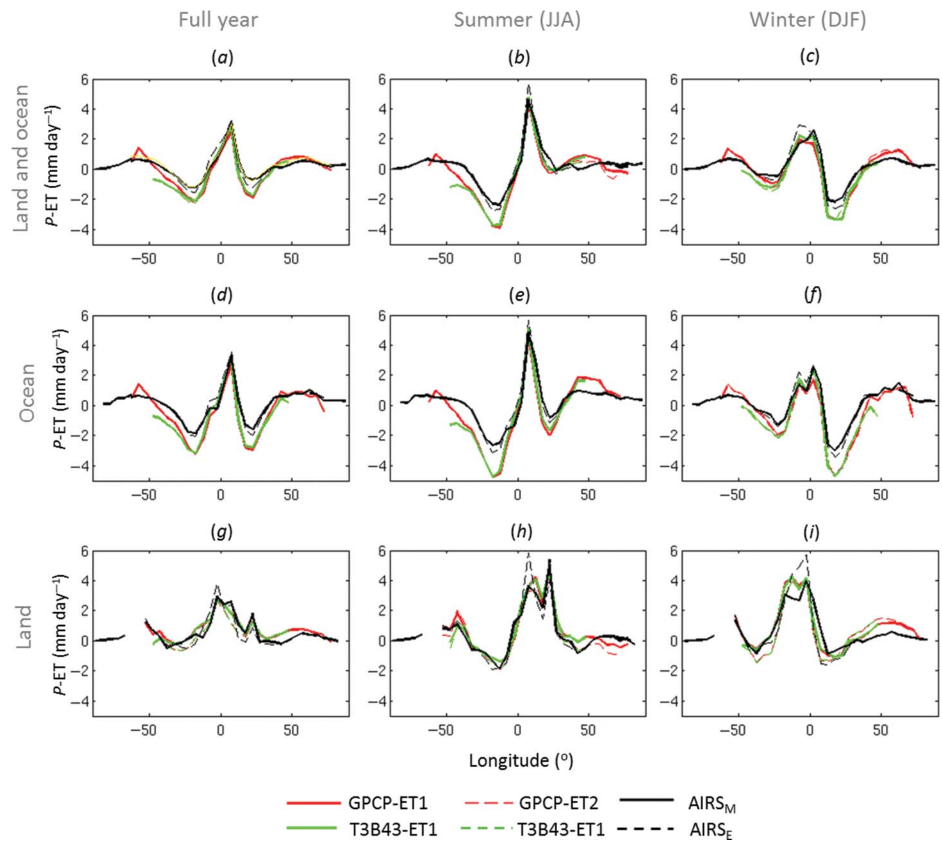

Figure 5. Zonal distribution of mean *P*–ET computed from $AIRS_E$, $AIRS_M$, GPCP-MOD16, GPCP-PT-JPL, T3B43-MOD16, and T3B43-PT-JPL for annual, winter, and summer over land and ocean, ocean, and land.

this difference is likely to be small (e.g. less than 0.3 mm day^{-1}; Behrangi et al. 2012). Furthermore, the analysis of Shie (2011) using available ship measurements over a reference station located at (20°S, 85°W) suggests that a positive bias of about 0.5 mm day^{-1} is possible from the GSSTF2c product. As ocean covers a much larger area than land and *P*–ET differences are relatively much smaller over land, similar patterns can be observed in the zonal difference for averaged land and ocean (top row panels). Over land (bottom row) the major differences are found over tropics (e.g. within 15°S–15°N) where $AIRS_E$ and $AIRS_M$ also show relatively large differences from the other data sets. Over the higher latitudes (e.g. poleward of latitude 40°), the observations of *P*–ET also show large differences compared to $AIRS_E$ and $AIRS_m$. This difference can be up to about 1 mm day^{-1} around 50°N over ocean in summer (Figure 5(*e*)) and over land in winter (Figure 5(*i*)). Both $AIRS_E$ and $AIRS_M$ are fairly consistent with each other in high latitudes, thereby making the analysis more conclusive in high latitudes. Note that the lack of ET data (e.g. poleward of latitude ~65°) hinders the full comparative analysis among different data sets and T3B43 is available up to only latitude 50° in both hemispheres. Although the two precipitation (GPCP and T3B43) and ET (MOD16 and PT-JPL) products may not fully agree at some regions (see Figure 2), the results discussed above are nonetheless valid (see Figure 5).

It is important to note that the accuracy of AIRS q can be impacted by the lack of sounding over opaque clouds as discussed in Fetzer et al. (2006) using column-integrated q from AIRS and AMSR-E. Although MERRA and ERA-interim assimilate AIRS radiance data, they provide complete fields of q even in the presence of cloudy opaque scenes. Figure 6 shows the annual, summer, and winter climatology maps of column-integrated water vapour sinks from MERRA and ERA (top two rows) and their differences with $AIRS_E$ and $AIRS_M$ (bottom two rows). $AIRS_M$ and $AIRS_E$ agree well with MERRA and ERA-interim, respectively, to produce the geographical distribution and seasonal cycle of *P*–ET, especially over ocean. This suggests that *P*–ET calculated from AIRS can be largely impacted by the differences in wind vectors from reanalysis, but much less by the lack of sounding over opaque clouds (Fetzer et al. 2006). Compared to MERRA, $AIRS_M$ shows smaller *P*–ET over the southern Amazon and north/northeast of Gulf of Alaska in summer. In contrast, $AIRS_M$ shows larger *P*–ET over Saudi Arabia in summer and tropical West Africa and southern China during winter. Figure 6 suggests that *P*–ET differences between $AIRS_E$ and ERA-interim are larger compared to that of $AIRS_M$ and MERRA over land. ERA-interim shows higher *P*–ET over tropical Africa and especially over the Tibetan Plateau and the surrounding regions in summer, which can exceed 2 mm day^{-1}. In winter, *P*–ET of ERA-interim exceeds that of $AIRS_E$ over broad regions in the north and centre of South America and the southern part of Africa. These could be related to the lack of sounding by AIRS over the opaque clouds as discussed above.

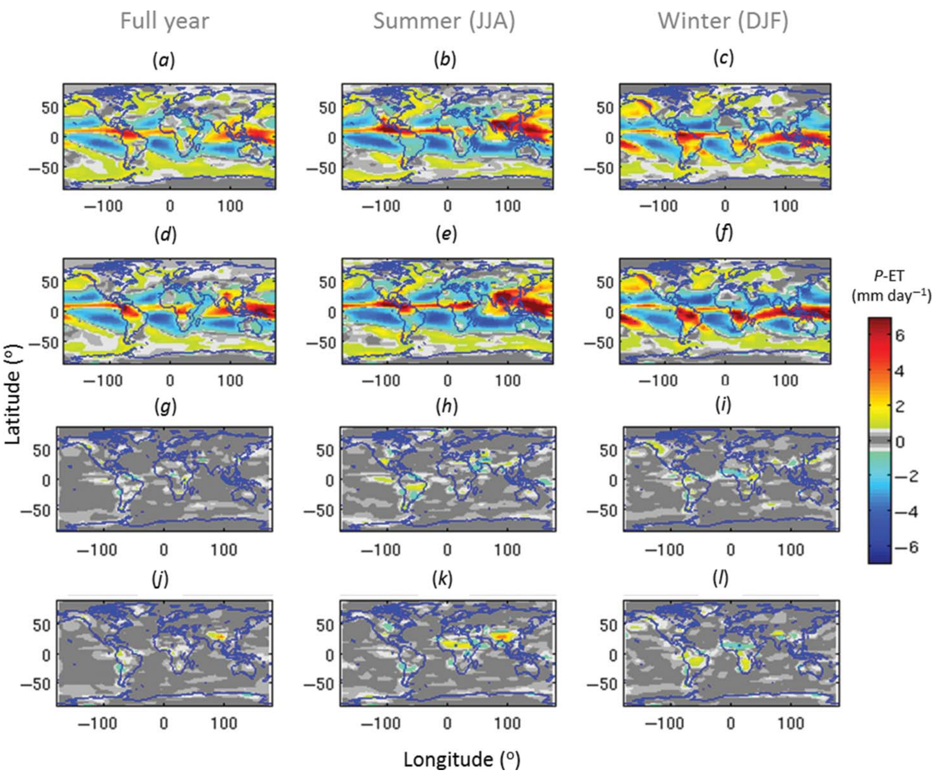

Figure 6. Climatology maps of column-integrated water vapour sinks from MERRA (*a*–*c*), ERA (*d*–*f*), and their differences with $AIRS_E$ (*g*–*i*) and $AIRS_M$ (*j*–*l*), respectively.

Table 1. Summary of the average *P*–ET values from different methods discussed in this study

	P–ET (mm day^{-1})					
	Land and ocean		Ocean		Land	
Method	Global	50°S–50°N	Global	50°S–50°N	Global	50°S–50°N
GPCP-ET1	–	–0.37	–	–0.86	–	0.88
GPCP-ET2	–	–0.43	–	–0.86	–	0.53
3B43-ET1	–	–0.41	–	–0.93	–	0.84
3B43-ET2	–	–0.47	–	–0.93	–	0.50
$AIRS_M$	0.18	0.10	0.04	–0.13	0.60	0.67
$AIRS_E$	0.14	0.05	0.02	–0.14	0.51	0.55
MERRA	0.23	0.13	0.06	–0.11	0.72	0.77
ERA-interim	0.20	0.07	0.05	–0.16	0.67	0.71

Table 1 summarizes the average water vapour sink and average *P*–ET values from different observations discussed in this study. The averaged values are reported over global and 50^{o}S–50^{o}N regions, separately over ocean, land, and both land and ocean. For fair comparison among different *P*–ET products, only grids with available values across all the products are considered in averaging within 50^{o}S–50^{o}N. In other words, regions with no ET data (see Figure 1) were removed from averaging. Over ocean within 50^{o}S–50^{o}N, averaged *P–E* from observed *P* (GPCP/T3B43) and observed *E* (GSSTF2c) range between –0.93 and –0.86 mm day^{-1}, but both showed larger negative number than the water vapour sinks from $AIRS_M$, $AIRS_E$, and reanalysis (range: –0.16 to –0.11 mm day^{-1}), consistent with Wong, Fetzer, Kahn, et al. (2011). This is consistent with Figure 5 (see subtropical oceans), where observed *P* minus observed *E* shows a larger negative number than those obtained from water vapour budget calculations. Averaged water vapour sinks from AIRS and reanalysis are also found to be consistent over global ocean and are close to zero (range: 0.02–0.06 mm day^{-1}). Over land, generally higher agreement between observed *P* minus observed ET and *P*–ET (calculated from AIRS and reanalysis) exists and all show positive values (range: 0.5–0.88). The average values over land and ocean lie between that of land-only and ocean-only with a slight positive global value (range: 0.14–0.23 mm day^{-1}), consistent with that found by Saha et al. (2010) using NCEP Climate Forecast System Reanalysis (CFSR).

4. Concluding remarks

Accurate quantification of *P*–ET has an important role in the calculation of land-atmosphere water balance and is critical for understanding the changes in global hydrologic and energy cycle in a changing climate. In the present study, global net surface water exchange (*P*–ET) rate is calculated and cross-compared using two independent approaches and various products collected between 2003 and 2006 based on the availability of all of the data sets. We used observed precipitation from GPCP and TRMM 3B43, ocean evaporation from GSSTF2c, and land ET from MOD16 and PT-JPL products to calculate the observed precipitation minus observed ET. We also calculated atmospheric column-integrated water vapour sink from water vapour budget equation using water vapour retrievals from the Atmospheric Infrared Sounder/Advanced Microwave Sounding Unit observation with wind fields from MERRA and ERA-interim (denoted $AIRS_M$ and

$AIRS_E$, respectively). The atmospheric water vapour sink is also obtained from the water vapour budget in MERRA and ERA-interim for consistency check with other products.

Using zonal plots and geographical maps, regions of main differences in the estimated surface water exchange are identified. Over ocean within 50°S–50°N latitudinal bounds, average surface water exchange from observed *P* (GPCP/T3B43) and observed *E* (GSSTF2c) ranged between –0.93 and –0.86 mm day^{-1}, but both showed a much larger negative number than that obtained from $AIRS_M$, $AIRS_E$, and reanalysis (range: –0.16 to –0.11 mm day^{-1}). Detailed analysis suggests that the differences mainly occurred over subtropical oceans, especially in the southern hemisphere in summer and the northern hemisphere in winter. Over land, generally higher agreement between observed *P* minus observed ET and atmospheric water vapour sinks (calculated from AIRS and reanalysis) is found, compared to the ocean. However, regions of large differences exist that are often season dependent. Averaged *P*–ET from AIRS and reanalysis is fairly consistent over global ocean and is close to zero (range: 0.02–0.06 mm day^{-1}) and ranges between 0.14 and 0.23 mm day^{-1} over global land and ocean.

It was also found that the pairs of $AIRS_M$ and $AIRS_E$ agreed well to produce the geographical distribution and seasonal cycle of atmospheric water vapour sink compared to using water vapour from MERRA and ERA-interim. This suggests that atmospheric water vapour sinks calculated from AIRS can be largely impacted by the choice of wind vectors from reanalysis, besides the lack of soundings over opaque clouds. Differences between the estimations of surface water exchange in the tropics to subtropics call for the need for further investigations and consistency check of satellite-based and reanalysis water vapour, reanalysis winds, precipitation observations, and surface evaporation estimates. In higher latitudes, atmospheric water vapour sinks calculated from $AIRS_M$, $AIRS_E$, MERRA, and ERA-interim are found to be more consistent with each other. This suggests that the atmospheric water vapour sink estimates can potentially be useful for consistency check between precipitation and ET products, especially in high latitudes where precipitation products face significant uncertainties (Adler, Gu, and Huffman 2012; Behrangi et al. 2012), rain gauges are sparse and often erroneous (Goodison, Louie, and Yang 1998), and observations of ET are significantly lacking. The analysis presented here can contribute to the evaluation of the moisture, wind, precipitation, and evaporation simulations from global climate models as well as climate reanalyses.

Acknowledgements

The research described in this article was carried out at the Jet Propulsion Laboratory, California Institute of Technology, under a contract with the National Aeronautics and Space Administration.

Funding

This study was supported by the JPL AIRS project and a contract with NASA. Funding to JBF was provided by NASA's Terrestrial Hydrology Program. Government sponsorship is acknowledged.

References

Adler, R. F., G. Gu, and G. J. Huffman. 2012. "Estimating Climatological Bias Errors for the Global Precipitation Climatology Project (GPCP)." *Journal of Applied Meteorology and Climatology* 51: 84–99. doi:10.1175/JAMC-D-11-052.1.

Adler, R. F., G. J. Huffman, A. Chang, R. Ferraro, P. P. Xie, J. Janowiak, B. Rudolf, U. Schneider, S. Curtis, D. Bolvin, A. Gruber, J. Susskind, P. Arkin, and E. Nelkin. 2003. "The Version-2 Global Precipitation Climatology Project (Gpcp) Monthly Precipitation Analysis (1979-present)." *Journal of Hydrometeorology* 4: 1147–1167. doi:10.1175/1525-7541(2003)004<1147:TVGPCP>2.0.CO;2.

Allen, M. R., and W. J. Ingram. 2002. "Constraints on Future Changes in Climate and the Hydrologic Cycle." *Nature* 419: 224–232. doi:10.1038/nature01092.

Anderson, M. C., J. M. Norman, J. R. Mecikalski, J. P. Otkin, and W. P. Kustas. 2007. "A Climatological Study of Evapotranspiration and Moisture Stress Across the Continental United States Based on Thermal Remote Sensing: 1. Model Formulation." *Journal of Geophysical Research* 112: D10117. doi:10.1029/2006JD007506.

Behrangi, A., M. Lebsock, S. Wong, and B. H. Lambrigtsen. 2012. "On the Quantification of Oceanic Rainfall Using Space Borne Sensors." *Journal of Geophysical Research* 117: D20105.

Behrangi, A., G. Stephens, R. F. Adler, G. J. Huffman, M. Lebsock. Forthcoming. "An Update on Oceanic Precipitation Rate and Its Zonal Distribution in Light of Advanced Observations from Space." *Journal of Climate*.

Bolvin, D. T., R. F. Adler, G. J. Huffman, E. J. Nelkin, and J. P. Poutiainen. 2009. "Comparison of GPCP Monthly and Daily Precipitation Estimates with High-Latitude Gauge Observations." *Journal of Applied Meteorology and Climatology* 48: 1843–1857. doi:10.1175/2009JAMC2147.1.

Bosilovich, M. G., F. R. Robertson, and J. Chen. 2011. "Global Energy and Water Budgets in MERRA." *Journal of Climate* 24: 5721–5739. doi:10.1175/2011JCLI4175.1.

Chou, S.-H., E. Nelkin, J. Ardizzone, R. M. Atlas, and C.-L. Shie. 2003. "Surface Turbulent Heat and Momentum Fluxes over Global Oceans Based on the Goddard Satellite Retrievals, Version 2 (GSSTF2)." *Journal of Climate* 16: 3256–3273. doi:10.1175/1520-0442(2003)016<3256:STHAMF>2.0.CO;2.

Dai, A., I. Y. Fung, and A. D. Del Genio. 1997. "Surface Observed Global Land Precipitation Variations During 1900–88." *Journal of Climate* 10: 2943–2962. doi:10.1175/1520-0442(1997)010<2943:SOGLPV>2.0.CO;2.

Dai, A., K. E. Trenberth, and T. Qian. 2004. "A Global Dataset of Palmer Drought Severity Index for 1870-2002: Relationship with Soil Moisture and Effects of Surface Warming." *Journal of Hydrometeorology* 5: 1117–1130. doi:10.1175/JHM-386.1.

Dee, D. P., S. M. Uppala, A. J. Simmons, P. Berrisford, P. Poli, S. Kobayashi, U. Andrae,M. A. Balmaseda, G. Balsamo, P. Bauer, P. Bechtold, A. C. M. Beljaars, L. van de Berg, J. Bidlot, N. Bormann, C. Delsol, R. Dragani, M. Fuentes, A. J. Geer, L. Haimberger, S. B. Healy, H. Hersbach, E. V. Hólm, L. Isaksen, P. Kållberg, M. Köhler, M. Matricardi, A. P. McNally, B. M. Monge-Sanz, J.-J. Morcrette, B.-K. Park, C. Peubey, P. de Rosnay, C. Tavolato, J.-N. Thépaut, and F. Vitart. 2011. "The ERA-Interim Reanalysis: Configuration and Performance of the Data Assimilation System." *Quarterly Journal of the Royal Meteorological Society* 137: 553–597. doi:10.1002/qj.828.

Divakarla, M., C. D. Barnet, M. D. Goldberg, L. M. McMillin, E. Maddy, W. Wolf, and L. Zhow. 2006. "Validation of AIRS Temperature and Water Vapor Retrievals with Matched Radiosonde Measurements and Forecasts." *Journal of Geophysical Research* 111: D09S15. doi:10.1029/2005JD006116.

Ferguson, C. R., J. Sheffield, E. F. Wood, and H. Gao. 2010. "Quantifying Uncertainty in a Remote Sensing-Based Estimate of Evapotranspiration Over Continental USA." *International Journal of Remote Sensing* 31: 3821–3865. doi:10.1080/01431161.2010.483490

Fetzer, E. J., B. H. Lambrigtsen, A. Eldering, H. H. Aumann, and M. T. Chahine. 2006. "Biases in Total Precipitable Water Vapor Climatologies from Atmospheric Infrared Sounder and Advanced Microwave Scanning Radiometer." *Journal of Geophysical Research* 111: D09S16. doi:10.1029/2005JD006598.

Fetzer, E. J., W. G. Read, D. Waliser, B. H. Kahn, B. Tian, H. Vömel, F. W. Irion, H. Su, A. Eldering, M. de la Torre Juarez, J. Jiang, and V. Dang. 2008. "Comparison of Upper Tropospheric Water Vapor Observations from the Microwave Limb Sounder and Atmospheric Infrared Sounder." *Journal of Geophysical Research: Atmospheres* 113 (D22): D22110.

Fetzer, E. J., J. Teixeira, E. T. Olsen, and E. F. Fishbein. 2004. "Satellite Remote Sounding of Atmospheric Boundary Layer Temperature Inversions Over the Subtropical Eastern Pacific." *Geophysical Research Letters* 31: L17102. doi:10.1029/2004GL020174.

Fisher, J. B., K. P. Tu, and D. D. Baldocchi. 2008. “Global Estimates of the Land-Atmosphere Water Flux Based on Monthly AVHRR and ISLSCP-II Data, Validated at 16 FLUXNET Sites.” *Remote Sensing of Environment* 112: 901–919. doi:10.1016/j.rse.2007.06.025.

Gettelman, A., E. M. Weinstock, E. J. Fetzer, F. W. Irion, A. Eldering, E. C. Richard, K. H. Rosenlof, T. L. Thompson, J. V. Pittman, C. R. Webster, and R. L. Herman. 2004. “Validation of Aqua Satellite Data in the Upper Troposphere and Lower Stratosphere with in Situ Aircraft Instruments.” *Geophysical Research Letters* 31: L22107. doi:10.1029/2004GL020730.

Goodison, B. E., P. Y. T. Louie, and D. Yang. 1998. *WMO Solid Precipitation Measurement Intercomparison, Rept*. Geneva: World Meteorological Organization, 67: 212.

Huffman, G. J., and D. T. Bolvin. 2012. *GPCP Version 2.2 Combined Precipitation Data Set Documentation*. Washington, DC: NASA Goddard Earth Sciences (GES), Data and Information Services Center (DISC). ftp://precip.gsfc.nasa.gov/pub/gpcp-v2.2/doc/V2.2_doc.pdf.

Huffman, G. J., D. T. Bolvin, E. J. Nelkin, D. B. Wolff, R. F. Adler, G. Gu, Y. Hong, K. P. Bowman, and E. F. Stocker. 2007. “The TRMM Multisatellite Precipitation Analysis (TMPA): Quasi-Global, Multiyear, Combined-Sensor Precipitation Estimates at Fine Scales.” *Journal of Hydrometeorology* 8: 38–55. doi:10.1175/JHM560.1.

Huffman, G. J., R. F. Adler, D. T. Bolvin, and G. Gu. 2009. “Improving the Global Precipitation Record: GPCP Version 2.1.” *Geophysical Research Letters* 36: L17808. doi:10.1029/2009GL040000.

Jiménez, C., C. Prigent, B. Mueller, S. I. Seneviratne, M. F. McCabe, E. F. Wood, W. B. Rossow, G. Balsamo, A. K. Betts, P. A. Dirmeyer, J. B. Fisher, M. Jung, M. Kanamitsu, R. H. Reichle, M. Reichstein, M. Rodell, J. Sheffield, K. Tu, and K. Wang. 2011. “Global Intercomparison of 12 Land Surface Heat Flux Estimates.” *Journal of Geophysical Research* 116: D02102. doi:10.1029/2010JD014545.

Mallick, K., B. K. Bhattacharya, V. U. M. Rao, D. R. Reddy, S. Banerjee, H. Venkatesh, V. Pandey, G. Kar, J. Mukherjee, S. P. Vyas, A. S. Gadgil, and N. K. Patel. 2009. “Latent Heat Flux Estimation in Clear Sky Days Over Indian Agro-Ecosystems Using Noontime Satellite Remote Sensing Data.” *Agricultural and Forest Meteorology* 149 (10): 1646–1665. doi:10.1016/j.agrformet.2009.05.006.

Monteith, J. L. 1965. “Evaporation and the Environment.” *Symposium of the Society of Exploratory Biology* 19: 205–234.

Mu, Q., F. A. Heinsch, M. Zhao, and S. W. Running. 2007. “Development of a Global Evapotranspiration Algorithm Based on Modis and Global Meteorology Data.” *Remote Sensing of Environment* 111: 519–536. doi:10.1016/j.rse.2007.04.015.

Mu, Q., M. Zhao, and S. W. Running. 2011. “Improvements to a MODIS Global Terrestrial Evapotranspiration Algorithm.” *Remote Sensing of Environment* 115: 1781–1800. doi:10.1016/j.rse.2011.02.019.

Mueller, B., S. I. Seneviratne, C. Jimenez, T. Corti, M. Hirschi, G. Balsamo, P. Ciais, P. Dirmeyer, J. B. Fisher, Z. Guo, M. Jung, F. Maignan, M. F. McCabe, R. Reichle, M. Reichstein, M. Rodell, J. Sheffield, A. J. Teuling, K. Wang, E. F. Wood, and Y. Zhang. 2011. “Evaluation of Global Observations-Based Evapotranspiration Datasets and IPCC AR4 Simulations.” *Geophysical Research Letters* 38: n/a–n/a. doi:10.1029/2010GL046230.

Peixoto, J. P., and A. H. Oort. 1992. “Physics of Climate.” *American Institute of Physics* 520. ISBN-10:0883187124.

Phillips, O. L., L. E. O. C. Aragao, S. L. Lewis, J. B. Fisher, J. Lloyd, G. Lopez-Gonzalez, Y. Malhi, A. Monteagudo, J. Peacock, C. A. Quesada, G. van der Heijden, S. Almeida, I. Amaral, L. Arroyo, G. Aymard, T. R. Baker, O. Banki, L. Blanc, D. Bonal, P. Brando, J. Chave, A. C. A. de Oliveira, N. D. Cardozo, C. I. Czimczik, T. R. Feldpausch, M. A. Freitas, E. Gloor, N. Higuchi, E. Jimenez, G. Lloyd, P. Meir, C. Mendoza, A. Morel, D. A. Neill, D. Nepstad, S. Patino, M. C. Penuela, A. Prieto, F. Ramirez, M. Schwarz, J. Silva, M. Silveira, A. S. Thomas, H. T. Steege, J. Stropp, R. Vasquez, P. Zelazowski, E. A. Davila, S. Andelman, A. Andrade, K.-J. Chao, T. Erwin, A. Di Fiore, C. E. Honorio, H. Keeling, T. J. Killeen, W. F. Laurance, A. P. Cruz, N. C. A. Pitman, P. N. Vargas, H. Ramirez-Angulo, A. Rudas, R. Salamao, N. Silva, J. Terborgh, and A. Torres-Lezama. 2009. “Drought Sensitivity of the Amazon Rainforest.” *Science* 323: 1344–1347. doi:10.1126/science.1164033.

Rienecker, M. M., M. J. Suarez, R. Gelaro, R. Todling, J. Bacmeister, E. Liu, M. G. Bosilovich, S. D. Schubert, L. Takacs, G. Kim, S. Bloom, J. Chen, D. Collins, A. Conaty, A. da Silva, W. Gu, J. Joiner, R. D. Koster, R. Lucchesi, A. Molod, T. Owens, S. Pawson, P. Pegion, C. R. Redder,

R. Reichle, F. R. Robertson, A. G. Ruddick, M. Sienkiewicz, and J. Woollen. 2011. "MERRA: NASA's Modern-Era Retrospective Analysis for Research and Applications." *Journal of Climate* 24: 3624–3648. doi:10.1175/JCLI-D-11-00015.1.

Saha, S., S. Moorthi, H.-L. Pan, X. Wu, J. Wang, S. Nadiga, P. Tripp, R. Kistler, J. Woollen, D. Behringer, H. Liu, D. Stokes, R. Grumbine, G. Gayno, J. Wang, Y. Hou, H. Chuang, H. H. Juang, J. Sela, M. Iredell, R. Treadon, D. Kleist, P. Van Delst, D. Keyser, J. Derber, M. Ek, J. Meng, H. Wei, R. Yang, S. Lord, H. Van Den Dool, A. Kumar, W. Wang, C. Long, M. Chelliah, Y. Xue, B. Huang, J. Schemm, W. Ebisuzaki, R. Lin, P. Xie, M. Chen, S. Zhou, W. Higgins, C. Zou, Q. Liu, Y. Chen, Y. Han, L. Cucurull, R. W. Reynolds, G. Rutledge, and M. Goldberg. 2010. "The NCEP Climate Forecast System Reanalysis." *Bulletin of the American Meteorological Society* 91 (8): 1015–1057. doi:10.1175/2010BAMS3001.1

Shie, C.-L. 2011. *Science Background for the Reprocessing and Goddard Satellite-Based Surface Turbulent Fluxes (Gsstf2c) Dataset for Global Water and Energy Cycle Research, Science Document for the Distributed Gddtf2c Via Goddard Earth Science (Ges) Data and Information Service Center (DISC)*, 19. Accessed October 28. http://disc.sci.gsfc.nasa.gov/measures/documentation/Science_of_the_data.GSSTF2c.pdf.

Shie, C.-L., L. Chiu, R. Adler, E. Nelkin, I. I. Lin, P. Xie, F.-C. Wang, R. Chokngamwong, W. Olson, and D. A. Chu. 2009. "A Note on Reviving the Goddard Satellite-Based Surface Turbulent Fluxes (GSSTF) Dataset." *Advances in Atmospheric Sciences* 26 (6): 1071–1080. doi: 10.1007/s00376-009-8138-z.

Stephens, G. L., J. L. Li, M. Wild, C. A. Clayson, N. Loeb, S. Kato, T. L'Ecuyer, P. W. Stackhouse, M. Lebsock, and T. Andrews. 2012. "An Update on Earth's Energy Balance in Light of the Latest Global Observations." *Nature Geoscience* 5: 691–696. doi:10.1038/ngeo1580

Sun, Y., S. Solomon, A. Dai, and R. W. Portmann. 2007. "How Often will it Rain?." *Journal of Climate* 20: 4801–4818. doi:10.1175/JCLI4263.1.

Susskind, J., C. Barnet, J. Blisdell, L. Iredell, F. Keita, L. Kouvaris, G. Molnar, and M. Chahine. 2006. "Accuracy of Geophysical Parameters Derived from Atmospheric Infrared Sounder/Advanced Microwave Sound Unit as a Function of Fractional Cloud Cover." *Journal of Geophysical Research* 111: D09S17. doi:10.1029/2005JD006272.

Susskind, J., P. Piraino, L. Rokke, L. Iredell, and A. Mehta. 1997. "Characteristics of the TOVS Pathfinder Path a Dataset." *Bulletin of the American Meteorological Society* 78: 1449–1472. doi:10.1175/1520-0477(1997)078<1449:COTTPP>2.0.CO;2.

Swenson, S. 2010. "Assessing High-Latitude Winter Precipitation from Global Precipitation Analyses Using GRACE." *Journal of Hydrometeorology* 11: 405–420. doi:10.1175/2009JHM1194.1.

Syed, T. H., J. S. Famiglietti, V. Zlotnicki, and M. Rodell. 2007. "Contemporary Estimates of Pan-Arctic Freshwater Discharge from GRACE and Reanalysis." *Geophysical Research Letters* 34: L19404. doi:10.1029/2007GL031254.

Tian, B., E. Manning, E. Fetzer, E. Olsen, and S. Wong. 2013. *AIRS/AMSU/HSB Version 6 Level 3 Product User Guide*, 37 p. Pasadena, CA: Jet Propulsion Laboratory/California Institute of Technology. http://disc.sci.gsfc.nasa.gov/AIRS/documentation/v6_docs

Tian, B., D. E. Waliser, E. J. Fetzer, B. H. Lambrigtsen, Y. L. Yung, and B. Wang. 2006. "Vertical Moist Thermodynamic Structure and Spatial–Temporal Evolution of the MJO in AIRS Observations." *Journal of Atmospheric Sciences* 63: 2462–2485. doi:10.1175/JAS3782.1.

Tian, Y., and C. D. Peters-Lidard. 2010. "A Global Map of Uncertainties in Satellite-Based Precipitation Measurements." *Geophysical Research Letters* 37: n/a–n/a. doi:10.1029/2010GL046008.

Tian, Y., C. D. Peters-Lidard, B. J. Choudhury, and M. Garcia. 2007. "Multitemporal Analysis of TRMM-Based Satellite Precipitation Products for Land Data Assimilation Applications." *Journal of Hydrometeorology* 8: 1165–1183. doi:10.1175/2007JHM859.1.

Trenberth, K. E., J. T. Fasullo, and J. Mackaro. 2011. "Atmospheric Moisture Transports from Ocean to Land and Global Energy Flows in Reanalyses." *Journal of Climate* 24: 4907–4924. doi:10.1175/2011JCLI4171.1.

Trenberth, K. E., L. Smith, T. T. Qian, A. Dai, and J. T. Fasullo. 2007. "Estimates of the Global Water Budget and its Annual Cycle Using Observational and Model Data." *Journal of Hydrometeorology* 8: 758–769. doi:10.1175/JHM600.1.

Vila, D., R. Ferraro, and R. Joyce. 2007. "Evaluation and Improvement of AMSU Precipitation Retrievals." *Journal of Geophysical Research-Atmospheres* 112: 14. doi:10.1029/2007JD008617.

Vinukollu, R. K., E. F. Wood, C. R. Ferguson, and J. B. Fisher. 2011. "Global Estimates of Evapotranspiration for Climate Studies Using Multi-Sensor Remote Sensing Data: Evaluation of Three Process-Based Approaches." *Remote Sensing of Environment* 115: 801–823. doi: 10.1016/j.rse.2010.11.006.

Wong, S., E. J. Fetzer, B. H. Kahn, B. Tian, B. H. Lambrigtsen, and H. Ye. 2011. "Closing the Global Water Vapor Budget with AIRS Water Vapor, MERRA Reanalysis, TRMM and GPCP Precipitation, and GSSTF Surface Evaporation." *Journal of Climate* 24: 6307–6321. doi: 10.1175/2011JCLI4154.1.

Wong, S., E. J. Fetzer, B. Tian, B. H. Lambrigtsen, and H. Ye. 2011. "The Apparent Water Vapor Sinks and Heat Sources Associated with the Intraseasonal Oscillation of the Indian Summer Monsoon." *Journal of climate* 24: 4466–4479. doi: 10.1175/2011JCLI4076.1.

Xie, P., and P. A. Arkin. 1997. "Global Precipitation: A 17-year Monthly Analysis Based on Gauge Observations, Satellite Estimates, and Numerical Model Outputs." *Bulletin of the American Meteorological Society* 78: 2539–2558. doi: 10.1175/1520-0477(1997)078<2539:GPAYMA>2.0.CO;2.

Yue, Q., E. J. Fetzer, B. H. Kahn, S. Wong, G. Manipon, A. Guillaume, and B. Wilson. 2013. "Cloud-State-Dependent Sampling in AIRS Observations Based on CloudSat Cloud Classification." *Journal of Climate* doi:. 10.1175/JCLI-D-13-00065.1.

Zelazowski, P., Y. Malhi, C. Huntingford, S. Sitch, and J. B. Fisher. 2011. "Changes in the Potential Distribution of Humid Tropical Forests on a Warmer Planet." *Philosophical Transactions of the Royal Society A: Mathematical, Physical and Engineering Sciences* 369: 137–160. doi: 10.1098/rsta.2010.0238.